ANALYSIS OF REPEATED ICESAT FULL WAVEFORM DATA: METHODOLOGY AND LEAF-ON / LEAF-OFF COMPARISON

Hieu Duong[1], Norbert Pfeifer[2] and Roderik Lindenbergh[1]

1: Delft University of Technology, Delft Institute of Earth Observation and Space systems, Delft, The Netherlands; (h.vanduong, r.c.lindenbergh)@lr.tudelft.nl
2: University of Innsbruck, Institute of Geography, Austria; norbert.pfeifer@uibk.ac.at

ABSTRACT

Analysis of the full waveform return pulse of laser altimeter systems is expected to increase the possibilities and accuracies in well-known applications of laser altimetry like forestry, digital terrain model generation, and earth surface analysis. In this study, at first, the ICESat full waveform data, which is acquired by NASA's ICESat Geoscience Laser Altimeter System (GLAS), is introduced and visualized. We analyze two epochs of data of the same groundtrack: the first epoch is recorded in the early winter season of 2003; the second contains data along the same track recorded at the end of the summer of the same year. First, the method of data analysis is discussed. The paper points out how to model the raw, noisy waveforms as a sum of Gaussian components obtained by a least square fit using suited parameters. The Gaussian components enable the decomposition of a full waveform into single constituent modes corresponding to certain reflecting objects within the laser footprint, for example tree canopy or ground surface. Moreover, normalization and shifting of the full waveform data is taken into account as well. This contribution contains the first investigation into the possibility of using repeated ICESat tracks to detect and describe changes in the forest area due to seasonal influences. Finally, results, possible error sources and future perspectives are discussed.

Keywords: ICESat, full waveform analysis, change detection, forestry

1 INTRODUCTION

ICESat stands for Ice, Cloud and land Elevation Satellite. ICESat was launched in January 2003 with the principal objectives to measure: polar ice-sheet elevation change; atmospheric profiles of cloud and aerosol properties; land topography profiles referenced to a global datum; and height of vegetation canopies. These objectives are accomplished using the Geoscience Laser Altimeter System (GLAS) combined with precise orbit determination. GLAS uses a laser altimeter to measure the range distance between the satellite and the earth surface. The instrument time stamps each laser pulse emission, and measures the echo pulse waveform from the surface. In fact, GLAS has 3 lasers on board, but laser 1 is not used anymore due to unexpected anomalies (NSIDC, 2005b). GLAS acquires elevation profiles of the entire earth consisting of 70m diameter footprints spaced every 175m along the profile. A waveform, recording laser back scatter energy as a function of time, is digitized for each footprint with a temporal resolution of 1ns.

As (Drake et al., 2002) put it: "[…] Forest canopy structure provides information about the primary surfaces of energy and matter exchange between the atmosphere and a major reserve of terrestrial aboveground carbon (Dixon et al., 1994). Knowledge of the total carbon content in […] vegetation provides a critical initial condition for studies […] which examine carbon flux caused by natural […] and anthropogenic […] processes. However, the accurate estimation of […] e.g., aboveground biomass […] of forest vegetation remains a major obstacle in conventional methods (Dubayah, 1997)."

The ICESat full waveform data gives new possibilities to extract more information about forest areas. The full waveform, digitized in 544 consecutive bins of 1ns over land (NSIDC, 2005a), corresponds to a vertical profile of energy returned from a reflecting area of 70m diameter. The land waveform 1ns sampling yields an 81.6m height range (544 waveform bins x 15cm/bin) of 15cm vertical resolution (Harding, 2005). Therefore, the waveform over forest area gives a multi-mode signal (Brenner et al., 2003), containing information about tree tops, crown thickness, canopy structure and ground surface.

Information on the forest structure can be extracted by means of a fitting algorithm which assumes that the waveform is a sum of Gaussian components. For ICESat the emitted waveform is a Gaussian and therefore the returning echo is a convolution of the vertically distributed scattering cross section with a Gaussian. For objects with homogeneous reflectivity this results in a Gaussian return if the scattering object is flat (horizontal or slanted) or has a Gaussian distribution of heights. Assuming this for the scatterers, as it is done in this paper, the Gaussian components of the echo bear information on the scatterers. Because no assumptions are made on the reflectivity or the size of the scatterers, only vertical characteristics can be inferred. The derived parameters of each Gaussian are used for extracting information on the forest structure. For example, the first Gaussian corresponds to a reflection from the tree canopy. A range from the first to the last Gaussain is a practical measure of tree height. The width of the first Gaussian is a measure of crown thickness. This is a justification for the decomposition. In addition, parameters derived from the Gaussian decomposition allow us to study deformation of the forest structure by considering changes in the parameter values.

In the next section we will first describe several processing steps that we used before we actually compare waveforms from different epochs. We explain how to standardize the waveforms via normalization and shift operations as well as how to fit the Gaussians to the waveforms. Then we introduce our comparison methods. In the results section we present our data set and give the results of the comparison between summer and winter waveforms. We finish with conclusions and remarks on further research. While the data used is from ICESat, the methods described below are more general.

2 METHODOLOGY

ICESat's data distribution consists of 15 data products called GLA01, GLA02, …, GLA15 (A. C. Brenner et al., 2003). In this study, we have investigated the products GLA01, which is the global full waveform data, and GLA14, the global land surface altimetry data. The GLA14 is a product obtained after precise geolocation, used here for visualizing the ICESat groundtracks, see Figure 4. The GLA01 is the product that contains the full captured waveform. This is the product that is used for our further waveform analysis. A GLA01 waveform is linked to a GLA14 location by index and shot number. The index and shot number are computed by relating the shooting time of an individual pulse to the starting time of the ICESat operation and the shooting frequency. ICESat full waveform data is distributed in binary format. We first converted it into ASCII format by an IDL program developed by the National Snow and Ice Data Center (the software/tools can be found at http://nsidc.org/data/icesat/tools.html, IDL_Readers). The waveform data that is originally in counts (from 0 to 255) is converted into voltage units for further analysis.

2.1 Waveform Normalization

The voltage waveform is then normalized. The purpose of the normalization is to enable comparison of waveforms, captured in different epochs. Due to e.g. different atmospheric conditions or changes in the behaviour of the laser device, the amount of energy in the laser return pulse may vary with time, even if the ground didn't change at all. These effects make it almost impossible to compare the absolute energy levels of particular constituents of different waveforms. The normalization step consist of dividing the received energy V_i at moment i by the total energy V_T, defined by $V_T = \sum_{i=1}^{544} V_i$. This implies that the area under any normalized waveform equals one. That is, the normalization is described as $V_N(i) = V_i / V_T$ .Two normalized full waveforms are shown in Figure 1.

2.2 Smoothing and initial parameter estimation

The voltage waveform is smoothed by a Gaussian filter. In this filter approach, weights for available observations are obtained by the relative height of a Gaussian shape at a observation location. The Gaussian shape is positioned such, that it maximum coincides with the filtering location. The width of the Gaussian shape is defined in terms of sigma. However, when the Gaussian is used for smoothing, it is usual to describe the width of the Gaussian with the Full Width at Half Maximum (FWHM). The FWHM is related to sigma by the formula:

FWHM = sigma * sqrt (8*log (2)).

We used a FWHM value of 3 for the smoothing step. The shape of the Gaussian is given by the normal distribution. After noise has been removed by the Gaussian filter, we can estimate the locations and amplitudes of the peaks in the smoothed waveform.

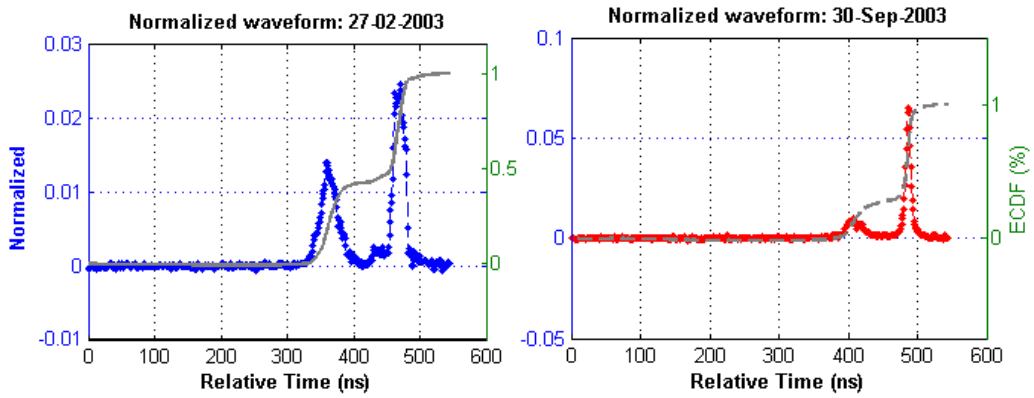

Figure 1: Two normalized waveforms from February, 2003 (on the left, blue) and from September, 2003 (on the right, red), are displayed together with their cumulative distribution curve (in gray).

Peak locations are estimated by a searching window 5 ns wide. The window moves from the beginning to the end of the waveform with an interval of 1ns. If the waveform value at the middle of the window is higher than at the four other window positions, and if moreover points on the left and the right are higher than the two outside points as well, the centre position is considered as the location of a peak. Then, the amplitude of the peak is extracted by the peak location in the voltage waveform. Finally, the width parameter or FWHM is calculated as a half distance between two neighbouring peaks. Moreover, the distance between neighbouring peaks is set to at least 5ns.

2.3 Fitting algorithm

In the fitting step, so-called Gaussian components are fitted to the normalized and smoothed waveform *w(t)*. Every Gaussian component W_m corresponds to one Gaussian bell curve. So, we assume that the smoothed waveform *w(t)* is a sum of Gaussian components W_m. That is, we write

$$w(t) = \sum_{m-1}^{N_p} W_m(t) \text{, with} \qquad W_m(t) = A_m e^{\frac{-(t-t_m)^2}{2\sigma_m^2}}$$

where *w(t)* is the amplitude of the waveform at time *t*, W_m (t) is the contribution from the *m*-th Gaussian component, N_p is the number of Gaussians found in the waveform, A_m is the amplitude of the *m*-th Gaussian, t_m its position and σ_m its standard deviation.

The least squares approach is used to compute the model parameters, that is, the values for A_m, t_m, and σ_m in the above equation are obtained by fitting the theoretical model to the observed waveform in such a way that the difference between model and observation is minimized in the least-squares sense. Two results of the fitting algorithm are shown in the Figure 4. The square sum of the residuals itself can be used to quantify the quality of the fit. And due to our normalization step this minimal sum and therefore the quality of the fit can be compared between the different waveforms.

In the following we will refer to the rightmost Gaussian component of the waveform decomposition as the *last mode,* as this mode corresponds to the energy reflected by the surface hit last. In forest applications, the last mode will in general correspond to the bare earth below the trees, as long as the earth surface is not completely hidden by vegetation. On the other hand, the leftmost Gaussian component is referred to as the first mode, as this component corresponds to the first feature in the laser footprint that is reflecting. Over forest area's, the first mode will mostly originate from reflection by the tree canopy.

Figure 2 shows the results of the fitting algorithm. On the left hand side the algorithm found four modes, on the right, in February, only two modes were found.

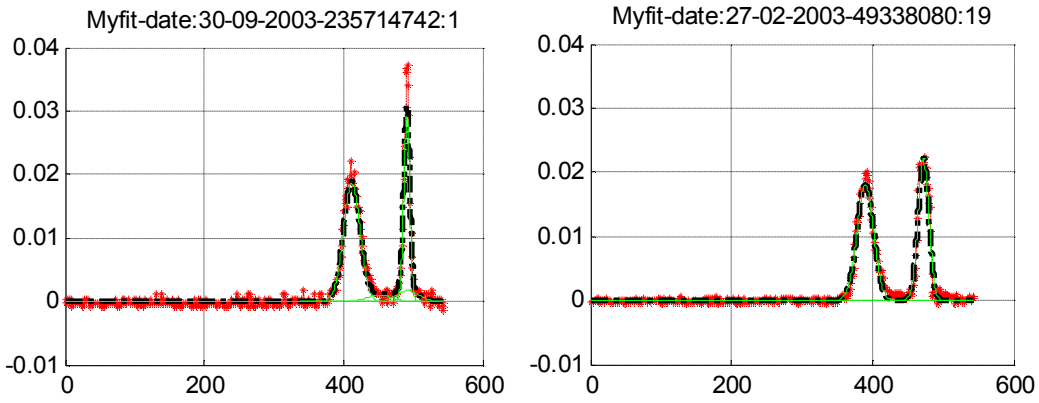

Figure 2: Two fitted waveforms (dashed black) are displayed together with the raw waveform (red) and the Gaussian components (green) for February, 2003 (left) and September, 2003 (right).

2.4 Shifting Computation

It appears that sometimes there occurs a shift error of the full waveform data between two epochs of data. The shift happens along the relative time axis, and could be caused by changes in the settings in the emitter/receiver unit of the GLAS instrument during the period in between the two epochs. Therefore, optimal shift parameters are computed in order to make the normalized waveforms better comparable along the y-axis. The shift computation is either applied on the complete waveform or on just the last mode of the waveform. The latter case is useful in case of rather different waveform shapes in the two epochs. In that case, the ground surface is still thought to be stable, which implies that the last modes of the two epochs should be matching.

The shift between two individual waveforms in two epochs is calculated by a cross correlation method. Due to the shift error, the waveform data of the second epoch is shifted to the left or the right in comparison to the first, or reference epoch. The shift error can be found by determining the cross-correlation $\hat{R}_{xy}(m)$ for time interval m, by

$$\hat{R}_{xy}(m) = \begin{cases} \sum_{n=0}^{N-m-1} x_{n+m} y_n^*, & m \geq 0 \\ \hat{R}_{yx}(-m), & m < 0 \end{cases}$$

This function returns the cross-correlation sequence as a length 2N-1 vector, where x and y are length N vectors (N>1). By determining that m that minimizes the length of the cross-correlation sequence $\left\| \hat{R}_{xy}(m) \right\|$, an optimal value for the shift is found. Note that in our case, N can be length of the entire waveform (N=544) or just the length of the last mode of the waveform (N≈100).

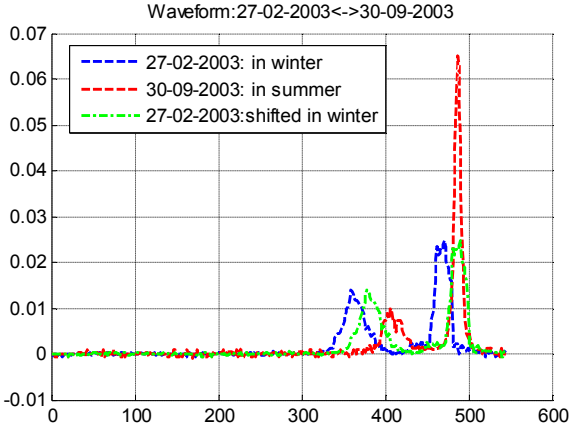

Figure 3: An original waveform in winter season (blue) is shifted to right (green) displayed with an original waveform in summer (red)

The shift operation is illustrated in Figure 3. The blue waveform is the one recorded in February; the red waveform is recorded at approximately the same location in September. It is clear that the two last modes don't match. As the terrain is very flat, this change cannot be caused by differences in the terrain height in the non-overlapping part of the respective footprints. Therefore a shift is determined with the cross-correlation method, which results in the, shifted, green February waveform. Now the last modes of the summer waveform and the shifted winter waveform do match.

2.5 Waveform deformation classes

After having applied the normalization and shifting operation, we are able to quantify the difference between a corresponding summer and winter waveform. Using these quantified differences, we divide the pairs of corresponding waveforms in four deformation classes.

The first class, class I, consists of pairs of waveforms that are very similar. Such correspondence occurs over flat areas with small or no vegetation and no buildings, like flat grass land or airports. Over such areas, the shift in the footprint location that we inevitable have, does not cause big changes in the waveform.

The last class, class IV, on the other end, contains pairs of waveforms that are incomparable, even if the footprints at least partially match. This happens over very inhomogeneous topography, like over cities, where a small change in the location of the 70m diameter footprint may exclude a part of a high building from being covered by the footprint in the second epoch.

The two remaining classes, classes II and III, are of more interest for forest applications. These two classes contain pairs of waveforms that are different, even after the normalization and shifting operation, but still somehow comparable. An example of such a pair was shown in Figure 3. Before distinguishing between classes II and III, two different notions of waveform distance are introduced first.

2.6 Waveform distances

Consider two corresponding waveforms, one waveform WF, from February and its corresponding waveform WS, from September, both normalized and, moreover, matched by the shift operation. For the comparison of WF and WS we introduce two notions: a feature based ratio and an intensity based distance. It should be noted however that the peak ratio is not a distance in the strict mathematical sense.

Above we have introduced the first mode and last mode of a waveform. Let LM denote the position of the peak of the last mode and FM the position of the peak of the first mode. The peak ratio RP compares the length between first and last mode in the two epochs, that is:

$$RP(W_F, W_S) = \begin{cases} \dfrac{LM_F - FM_F}{LM_S - FM_S} - 1, & LM_F - FM_F > LM_S - FM_S \\ \dfrac{LM_S - FM_S}{LM_F - FM_F} - 1, & LM_F - FM_F \le LM_S - FM_S \end{cases}$$

Note that this ratio is computed along the x-axis. Moreover it should be noted that the absolute location of the peaks of the nodes is not important here, just the location of the first peak relative to the location of the last peak.

The intensity distance on the other hand is determined along the y-axis and equals the mean squared distance between the relative intensities of the February waveform and the September waveform:

$$DI(W_F, W_S) = \sum_{i=1}^{544} \frac{(V_F(i) - V_S(i))^2}{544}$$

These two distances like notions are used to classify pairs of Summer/Winter waveforms into four deformation classes. For a leaf forest for example, the peak ratio distance between summer and winter maybe close to 0, but the intensity distance will significantly differ from 0, as the width of the first mode in September will be considerably wider. We define a distance as *small* if a distance is between the 25% shortest distances between pairs of waveforms. As we have two distances we obtain four differ-

ent classes: Class *same:* both RP and DI are small, Class *not comparable:* both RP and DI are not small; Class *strong change:* RP small but DI not small*;* Class *slight change*: RP not small but DI small. The class names 'strong change' and 'slight change' do not necessarily resemble specific tree types, but is indicative of forest types found in this region. The interest lies in the automatic classification itself.

3 RESULTS AND DICUSSION

3.1 Test forest data

The data we analysed belongs to a track covering part of The Netherlands, Belgium, Luxembourg and France. The ICESat data used in this area is from two epochs, one from 27-02-2003 (winter season, 1840 waveforms) and the other from 30-09-2003 (end of summer season, 2942 waveforms). The GLA14 is used to visualize the geolocation of the waveform data which appears as a straight red line in Figure 1. Actually, it consists of approximately circular footprints of 70m diameter with an inter-footprint spacing of 175m. The data of the two epochs are overlapped and displayed in one global view. Therefore, in the figure only one track is visuable, -but actually there are two tracks.

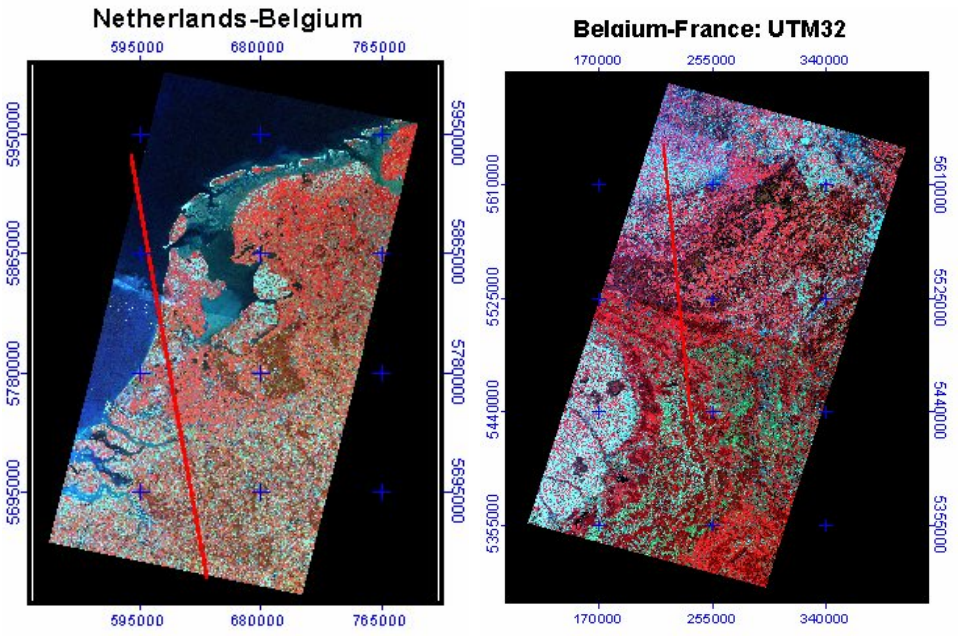

Figure 4: ICESat groundtracks from February and September 2003 overlayed on LANDSAT false colour image. As both tracks almost coincide, they appear as one track in the image.

The ICESat groundtracks are visualized together with 30m-LANDSAT images which are false colour composition. The LANDSAT images over the Netherlands, Belgium and the north of France were acquired in 2001 and 2000. The LANDSAT images were used to manually select waveform data from forest areas. Based on visual interpretation we selected 358 waveforms over forest. These data do not cover one big forest but rather several smaller patches of different kind of forest, including both pine and deciduous forest.

3.2 Footprint shifts

The repeated tracks do not overlap completely; the actual corresponding footprints of two epochs are shifted 73.8m in average. This causes inaccuracy in change detection in forest areas. However, if the area is a homogeneous forest, we may assume that similar waveforms are returned from all over the area, and moreover, we can detect seasonal changes in the forest structure by analyzing changes from even not fully overlapping footprints. In the above Figure, the red ellipse footprint is data tracked in September 2003, the green footprints are from February 2003.

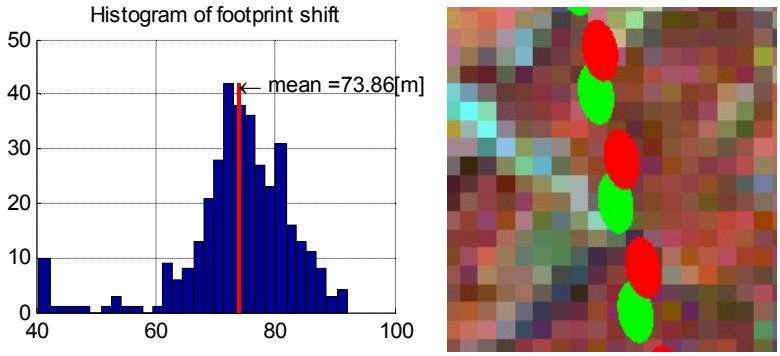

Figure 5: Histogram of footprint shift and its mean (of left), visualization of footprint shift (on right) with 30m Landsat images. Footprint size of 53 x 97m (Abshire et al. 2005)

3.3 Intensity comparison.

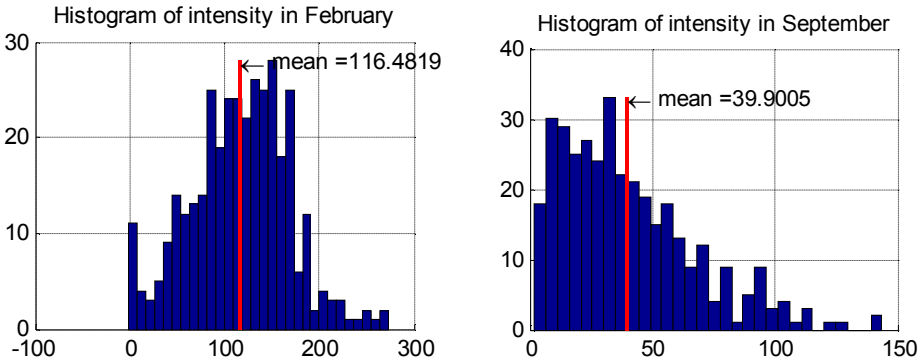

Figure 6: Mean intensity for February and September Waveform on left and right, respectively

The intensity or the full returned energy of waveform data in February is much larger than in September. This is illustrated in Figure 6, where histograms of the intensities in February and in September are given. The mean intensity differs by almost a factor 3. One of the reasons for this difference is the change of GLAS sensor L1 to sensor L2 aboard of the ICESat satellite. This implies that we cannot directly compare waveforms from the two different seasons. Therefore, relative intensities only should be considered in the further classifications steps.

3.4 Peak location, peak amplitude and shift distance

The first-last peak distance in winter and summer are comparable. In February the average distance equals 20.41 [m], in September it is 19.18 [m]. This difference could be explained by changes in the width of the modes between the seasons.

Above, we have introduced two methods for matching corresponding waveforms. The first method takes the full waveforms into account and with this method we find a mean shift of 4.26[m] downwards for the February waveform to match it optimally with the September waveform. If we match using the last mode only, we find a mean downwards shift of 4.84 [m]. These two shift values are comparable in size, but still they differ more then half a meter. Moreover, the size of the shifts found, shows that such a shift operator is really necessary. Again the reason for this big shift may be found in the change of sensor used aboard of the ICESat satellite.

The amplitude of the first mode in February is considerably lower than in September, see Figure 7. The mean first mode amplitude in winter equals 0.00418, in summer we found a value of 0.0056. This is probably caused by the more dense crowns of the trees in summer. The amplitudes of the last mode in summer and winter turn out to be quite similar, 0.0083 in winter versus 0.0088 in summer. This means that the ground surface is not changed much.

Except for the amplitudes, we also considered the width of the first and last modes. Again the differences for the last mode are small, but for the first mode we found a mean sigma of 4.28 [m] in win-

ter and a mean sigma of 3.74[m] in summer. We do not have a good explanation for this difference, but it may be possible that in summer the first mode is often more restricted to the tree crowns, while in winter the first mode widens, and incorporates larger parts of the trees.

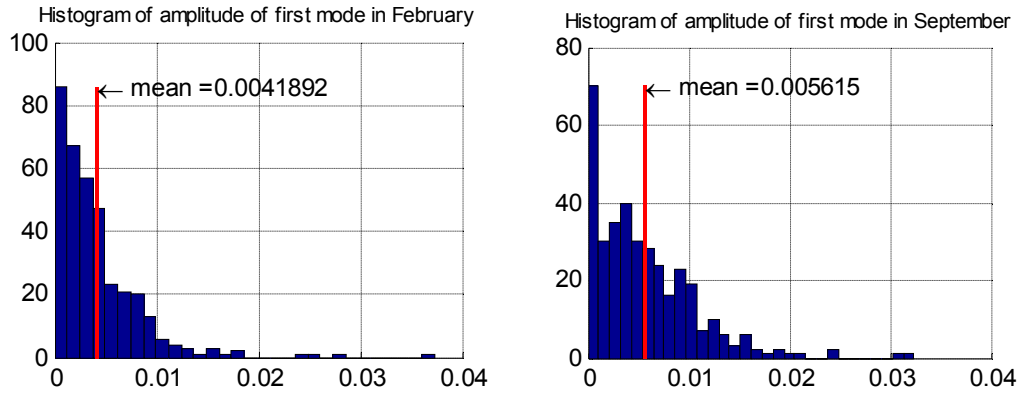

Figure 7: Average amplitude last/first mode February and September

3.4.1 Waveform distances

For about 358 pairs of summer-winter waveforms we determined both the Intensity Distance *DI* and the Peak Ratio *RP*. Based on the distances found we choose two critical threshold values *C_DI* and *C_RP*. These are both defined as the 0.25 quantile of the distances found. This procedure gives us for *C_DI* a value of 2.18e-6 and for *C_RP* a value of 0.12.

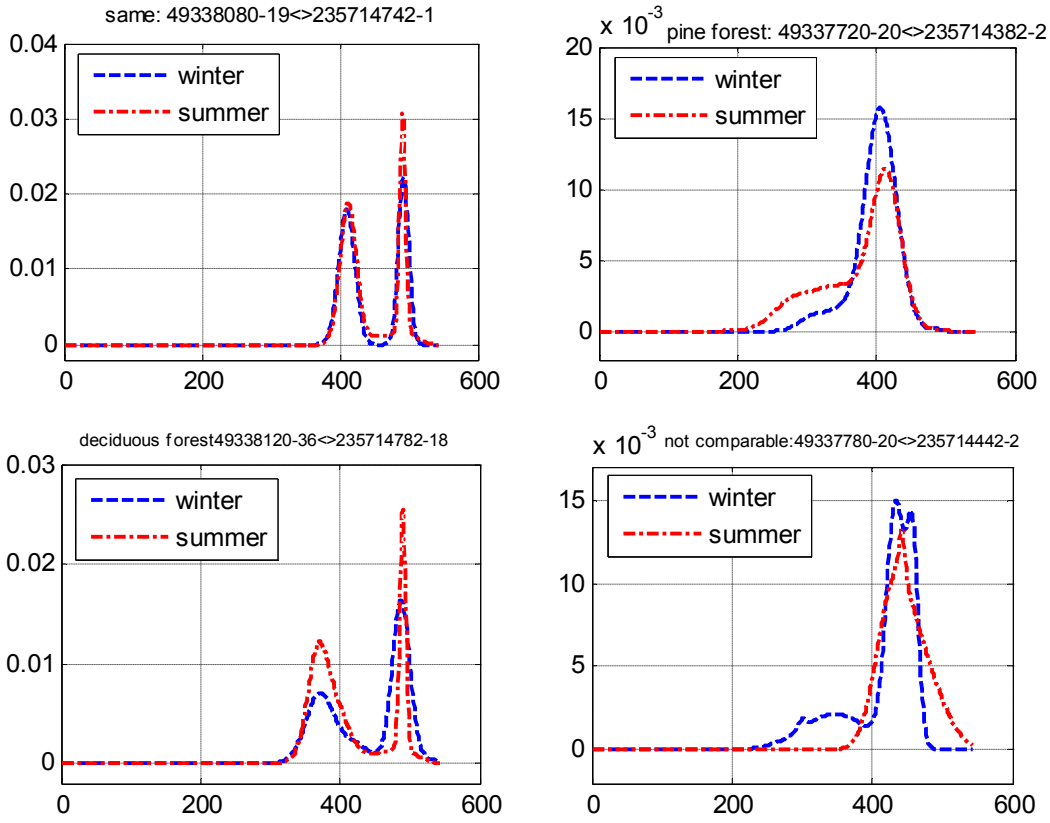

Figure 8: Four representative pairs of waveforms in four different classes: same (top left), slight change (maybe pine forest, top right), strong change (maybe deciduous forest, bottom left), and not comparable (bottom right)

If an intensity distance *DI* is smaller then *C_DI*, it is defined to be *small*, and similarly for *C_RP*. These two critical values allow us to divide the 358 pairs in the four deformation classes as introduced above. For each of the four classes representatives are shown in Figure 8.

There are 20 pairs of waveform in the class of *same*, 69 pairs in the class of *slight change*, 70 pairs in the class of *strong change* and 199 pairs in the class of *not comparable*.

The class of *slight change* contains pairs of waveform with *RP small* and *DI not small*, implying a change in waveform along the laser ray. Such changes could be caused by tree crowns that are getting larger in diameter; this class is useful for extracting and monitoring the canopy structure.

The class of *strong change* contains pairs with *DI small* and *RP not small*, implying a change in the height of the forest. This class is useful for monitoring or measuring the growth patch of trees in the forest.

The class of *same* contains pairs of similar waveforms. Here the forest is neither changing much in height (from February to September of the same year 2003) nor in foliage

The class of *not comparable* contains pairs of waveforms that are quite different. One of the reasons for such differences may be the appearance of new artificial objects like buildings within the footprints.

4 CONCLUSIONS AND FURTHER RESEARCH

The dataset we considered was far from ideal: the forest is not homogeneous, while the instruments used for the data acquisition differed between the two epochs. Still we were able to find considerable differences between the summer and winter data.

It seems like there are big differences in the intensities returned from forest and non-forest areas. In general, the intensities from forest areas are much lower. It would be interesting to quantify these differences and to investigate whether it is possible to use the results for enhancing classification or deformation detection and analysis methods.

In this paper we first identified some parameters that can be extracted from waveform data. In the next step we started to analyze changes in the parameter values. Further research could focus on identifying those parameters that are most significant for certain forest properties, like relative intensity of the returned signal, or ratio between the relative intensities of the first and the last mode. After identification of these parameters, a more sophisticated ‘waveform distance’ could be defined.

ACKNOWLEDGEMENTS

We would like to thank the National Snow and Ice Data Center for their data distribution. This project is funded by the Delft Research Centre ‘Earth’.

REFERENCES

Abshire, J. (2005). Geoscience Laser Altimeter System (GLAS) on the ICESat Mission: On-orbit measurement performance, Geophys. Res. Lett., doi:10.1029/2005GL024028, in press.

Brenner, A. C. (2003). Geoscience Laser Altimeter System Algorithm Theoretical Basis Document: Derivation of Range and Range Distributions from Laser Pulse Waveform Analysis, 92 pp. available at http://www.csr.utexas.edu/glas/atbd.html last visited on February 22, 2006

Dixon, R. K., Brown, S., Houghton, R. A., Solomon, A. M., Trexler, M. C., and & Wisniewski, J. (1994). Carbon Pools and Flux of Global Forest Ecosystems. Science, 263: 185-190.

Drake, J. B, et al (2002). Estimation of tropical forest structural characteristics using large-footprint lidar. Remote Sensing of Environment 79: 305– 319.

Dubayah, R., Blair, J. B., Bufton, J. L., Clark, D. B., JaJa, J., Knox, R. G., Luthcke, S. B., Prince, S., & Weishampel, J. F. (1997). The Vegetation Canopy Lidar mission. Land Satellite Information in the Next Decade II: Sources and Applications. American Society for Photogrammetry and Remote Sensing, Bethesda, MD, pp 100-112.

Harding, D. J. (2005). ICESat waveform measurements of within-footprint topographic relief and vegetation vertical structure. Geophysical Research Letters, 32, L21S10, doi:10.1029/2005GL023471.

National Snow and Ice Data Center (2005a). Frequently Asked Question, http://nsidc.org/data/icesat/faq.html, last visited on February 22, 2006.

National Snow and Ice Data Center (2005b). ICESat mission status. News, http://nsidc.org/data/icesat/news.html, last visited on February 22, 2006.